Vertical eddy diffusion and nutrient supply to the surface mixed layer of the Antarctic Circumpolar Current

C. S. Law,[1,2] E. R. Abraham,[3] A. J. Watson,[4] and M. I. Liddicoat[1]

Received 19 August 2002; revised 10 December 2002; accepted 12 May 2003; published 22 August 2003.

[1] Dispersion of the tracer sulphur hexafluoride (SF_6) during the Southern Ocean Iron Enrichment Experiment (SOIREE) provided an estimate of vertical exchange at the base of the surface mixed layer (60 m) at 61°S 140°E. Budget analysis confirmed that the SF_6 patch was well constrained by surface mapping, with the decline in total SF_6 showing good agreement with that predicted from wind speed parameterizations. Two approaches were used to calculate the mean effective vertical diffusivity *Kz* from the diapycnal transfer of SF_6, with complementary error function and second-moment fits to the SF_6 depth profiles indicating that *Kz* was less than 0.3×10^{-4} m^2s^{-1}. This result was examined using a three-dimensional diffusion model that incorporated lateral dispersion and air-sea exchange losses, which confirmed that vertical shear and subpycnocline dispersion did not influence the *Kz* estimate. Current shear at the base of the mixed layer was generated by wind-driven inertial oscillation, with a decrease in wind speed and increasing stratification in the latter half of the experiment reducing diapycnal transfer of SF_6. A compilation was used to examine the potential of both *N* (Brunt-Väisälä frequency) and *Ri* (gradient Richardson number) on the basis of parameterizations of *Kz* in the seasonal pycnocline. Application of *Kz* to nutrient gradients in the seasonal pycnocline suggests that vertical diffusion represents a significant pathway for silicic acid supply in late summer. Furthermore, use of the mean effective *Kz* ($0.11 \pm 0.2 \times 10^{-4}$ m^2s^{-1}) indicates that vertical diffusion supplies a large proportion of the iron required for new production in this region. *INDEX TERMS:* 4207 Oceanography: General: Arctic and Antarctic oceanography; 4568 Oceanography: Physical: Turbulence, diffusion, and mixing processes; 4572 Oceanography: Physical: Upper ocean processes; 4808 Oceanography: Biological and Chemical: Chemical tracers; 4845 Oceanography: Biological and Chemical: Nutrients and nutrient cycling; *KEYWORDS:* tracer, vertical diffusion, pycnocline, nutrients, iron, phytoplankton

Citation: Law, C. S., E. R. Abraham, A. J. Watson, and M. I. Liddicoat, Vertical eddy diffusion and nutrient supply to the surface mixed layer of the Antarctic Circumpolar Current, *J. Geophys. Res.*, *108*(C8), 3272, doi:10.1029/2002JC001604, 2003.

1. Introduction

[2] Vertical diffusion contributes to the maintenance of the heat, momentum and salt budgets of the ocean, and facilitates the transport and partitioning of carbon, nutrients, trace gases and anthropogenic substances between the surface and deep ocean. The rate of diapycnal diffusion in the main thermocline is relatively small compared to mixing along isopycnal surfaces which although scale-dependent is at least four orders of magnitude greater [*Ledwell et al.*, 1993, 1998]. This difference arises from the scale of the associated features, with isopycnal exchange constrained by the size of eddies, and diapycnal exchange controlled by stratification and cm-m turbulence scales. Nevertheless, diapycnal exchange represents a significant route for nutrient supply for new production, particularly in oligotrophic regions where the vertical nitrate flux effectively constrains carbon uptake [*Lewis et al.*, 1986]. Although the focus of most studies of nutrient exchange has been the permanent thermocline, the seasonal pycnocline is the primary boundary between nutrient deficit and excess during the phytoplankton growth season. The sharp gradient at this interface and proximity to high nutrient concentrations highlights the significance of this source to phytoplanktonic nutrient requirements, particularly at sites where location or hydrography preclude or minimize other sources such as frontal exchange, upwelling, runoff, and aeolien input.

[3] The mechanisms driving this exchange and so determining diapycnal diffusivity are not fully understood. Energy transfer at the ocean surface is modulated by surface waves, currents and internal waves, and dissipated along a progressive gradient of scales from large episodic events, such as upwelling and storm events, to the molecular dissipation of heat. Diapycnal diffusion across the seasonal

[1]Plymouth Marine Laboratory, Plymouth, UK.
[2]Now at National Institute for Water and Atmospheric Research, Wellington, New Zealand.
[3]National Institute for Water and Atmospheric Research, Wellington, New Zealand.
[4]School of Environmental Sciences, University of East Anglia, Norwich, UK.

0148-0227/03/2002JC001604

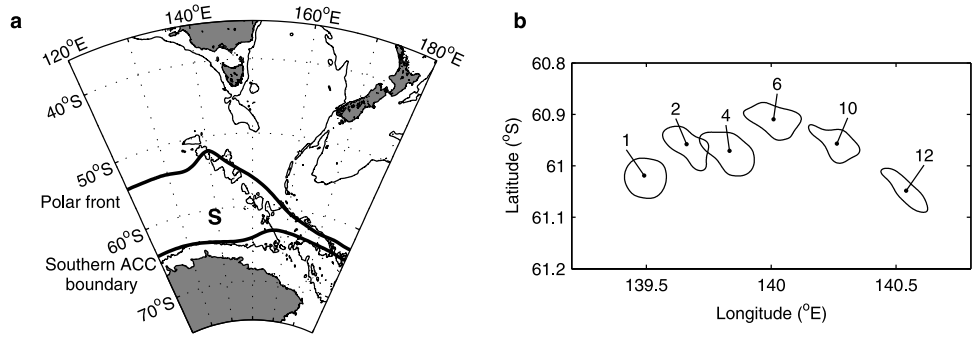

Figure 1. (a). Map of Australasian sector of the Southern Ocean showing the position of the SOIREE SF_6 release (S). The relative positions of the Polar front and southern ACC boundary are also included. (b). The lateral evolution of the SF_6 patch as indicated by the 50 fmol/L SF_6 contour on selected days during SOIREE.

pycnocline in the open ocean occurs predominately via small-scale turbulent processes that have been investigated primarily by microstructure measurements. These measurements have provided insight into the underlying mechanisms, but have inherent uncertainties in mixing coefficients and limitations of scale. Mixing in the upper ocean is dominated by infrequent significant events that are too intermittent to be adequately documented by this approach [*Gregg*, 1987]. An alternative approach to quantifying diapycnal diffusion in the open ocean is via the penetration of the tracer sulphur hexafluoride (SF_6) across the seasonal pycnocline. This provides an estimate of the effective diffusivity K_z that is an integrated measure over all turbulent events during the observation period [*Law et al.*, 1998, 2001]. Results from these studies have been used to examine the potential for a global parameterization of K_z in the seasonal pycnocline [*Law et al.*, 2001]. As ocean general circulation models are highly sensitive to vertical diffusivity [*Bryan*, 1987], a robust parameterization for K_z is a critical prerequisite for realistic modeling of upper ocean exchange and biogeochemical budgets, and in understanding their sensitivity and response to climate variability.

[4] Although nitrogen supply, in the form of nitrate, has been the primary focus of carbon export studies, it has become apparent over the last decade that in certain regions (referred to as high-nutrient low-chlorophyll (HNLC)), export is instead limited by iron availability [*Martin and Fitzwater*, 1988]. In contrast to nitrogen, for which availability varies predominately on seasonal timescales, the availability of iron in the surface ocean is dictated by its redox state. Although deep mixing during winter elevates iron availability in surface waters [*de Baar et al.*, 1995; *Watson et al.*, 2000], the open ocean supply is primarily determined by intermittent and localized events such as dust deposition, upwelling and frontal advection [*de Baar and Boyd*, 2000]. Estimates of these sources have been obtained by both direct measurement and modeling [*Bowie et al.*, 2001; *Fung et al.*, 2000], but the diffusive supply that maintains a relatively constant "background" supply of iron to the surface ocean has received little attention. The primary aim of the Southern Ocean Iron Enrichment Experiment (SOIREE) at 61°S 140°E (see Figure 1a) in February 1999 was to examine whether the availability of the micronutrient iron determines phytoplankton community structure, and limits carbon export in the Southern Ocean, the largest of the HNLC regions [*Boyd et al.*, 2000; *Boyd and Law*, 2001]. SOIREE also provided an opportunity to assess and compare natural routes of supply and internal cycling of iron [*Bowie et al.*, 2001; *Maldonado et al.*, 2001]. The experimental framework for SOIREE was a Lagrangian SF_6/iron release [*Watson et al.*, 1991; *Law et al.*, 1998], in which SF_6 provided a label for the enriched patch and a proxy for the iron when no longer detectable. Consequently this experiment also provided an opportunity to obtain a first estimate of the effective diffusivity across the seasonal pycnocline of the deep surface mixed layer (~60 m), in the dynamic and meteorologically energetic Antarctic Circumpolar Current (ACC). In addition, the concurrent measurement of K_z and nutrient gradients at the base of the seasonal mixed layer permitted determination of the vertical flux of potentially limiting nutrients, such as iron and silicic acid, and assessment of the importance of this pathway in supporting phytoplanktonic nutrient requirements.

2. Methods

[5] The tracer sulphur hexafluoride (SF_6) and acidified iron (II) were added to the surface mixed layer from the R/V *Tangaroa* to an area of 50 km^2, and the patch was subsequently followed for a period of 13 days (see Figure 1b). Ignoring evasive losses the SF_6 tracer is conservative, and provides a Lagrangian capability that minimizes the influence of surface currents and advection that can confound interpretation within Eularian studies. The response of the biota and biogeochemistry to the iron addition was determined by comparison of vertical profiles at the patch centre (IN stations), as identified by the SF_6 signal, with stations >8 km outside the patch boundary (OUT stations).

[6] The preparatory and analytical routines for SF_6 saturation and underway analysis are described by *Upstill-Goddard et al.* [1991]. In brief ~165 gms of SF_6 was dissolved in surface seawater in a 4000 L steel tank and subsequently released into surface waters at a rate of ~300 L/hr. The volume of the displaced SF_6-saturated water was replaced by surface seawater which filled a meteorological balloon in the top of the tank, so reducing SF_6 evasion [*Law et al.*, 1998]. The SF_6 and iron (II) solution were mixed in an SF_6/iron molar ratio of ~1.2 ×

10^{-4}, and expelled through reinforced tubing over the aft of the vessel over a period of 12 hours. The outlet was maintained at a depth of ~15 m by attachment to a depressor, with the release undertaken at a ship speed of 2–3 knots. The release was coordinated in a Lagrangian framework by reference to a drogued GPS buoy that marked the nominal centre of the patch, with buoy position updates transmitted to the ship at 10 min intervals by a UHF packet radio. The release track described an expanding hexagonal spiral with a between-track distance of ~600 m.

[7] Following a period of 6 hours to allow for mixing of the SF_6 and iron (II) the horizontal distribution of the surface SF_6 was surveyed using an underway analysis system. SF_6 was stripped from seawater from the ships intake at 5 m depth, with subsequent cryogenic trapping, chromatographic separation and detection by electron capture detector [*Law et al.*, 1998], with a measurement every 2.75 min and spatial resolution of 0.43–0.85 km at a ship speed of 5–10 knots. Near real-time display of the surface SF_6 distribution in the earth coordinates was obtained by integrating the SF_6 measurement with the ships GPS position, so enabling identification and location of the SF_6 patch boundaries and centre. The surface SF_6 data were reinterpreted postcruise using the drifter buoy positional data and ADCP data to provide a Lagrangian correction for SF_6 budgets and estimates of lateral dispersion [*Abraham et al.*, 2000].

[8] SF_6 vertical profiles were obtained to a depth of 160 m at 11 IN stations, with the majority of stations characterized by 3 separate casts. Vertical profiles were also obtained at 6 OUT stations during the experiment and 6 OUT stations during a final transect on day 13. Duplicate water samples of 500 mL were collected for each depth from Niskin bottles, maintained at in situ temperatures and analyzed within 2 hours of collection. The discrete SF_6 analytical system was similar to the underway system, but with the inclusion of an initial vacuum stage that accommodates water sample introduction and accelerates the stripping process [*Law et al.*, 1994]. Analytical sensitivity was ~0.04 fmol/L with a reproducibility for duplicate analysis of 1.6%. The stripping efficiency of the underway SF_6 system was primarily influenced by the seawater and gas flow rates, and was independent of tracer concentration. Comparison with water samples analyzed by the discrete system indicated that trapping efficiency of the mapping system always exceeded 90%.

[9] Dissolved nutrient and iron concentrations at the OUT stations are reported by *Frew et al.* [2001] and *Bowie et al.* [2001]. Wind speed data was collected by an anemometer attached to the ships mast at a height of 15 m and corrected to 10 m for thermal stability effects by reference to equivalent wind speed at 10 m, on the assumption of neutral air boundary conditions [*Large and Pond*, 1982]. The wind data was not corrected for any artifactual influence of the anemometer position, although recent fluid dynamic modeling of the flow field around the R/V *Tangaroa* indicates that measurements on the mast may be subject to a mean flow distortion of 15% (S. Popinet, personal communication).

[10] Stability of the water column was expressed by the Brunt-Väisäla frequency, N, using the equation:

$$N^2 = (g/\rho_0)(\Delta\rho/\Delta z) \quad (1)$$

where g is acceleration due to gravity, ρ_0 is reference density and $\Delta\rho/\Delta z$ is the density gradient over depth interval Δz. A hull-mounted 150 kHz RD instruments Acoustic Doppler Current Profiler (ADCP) was used to measure current velocity beneath the ship. A GPS and motion sensor system provided a correction for the ships motion for absolute velocities. The data was collected in 8 m depth bins, with the uppermost bin centered at 27 m depth. Velocity profiles were obtained at 10 min intervals, although there were data gaps where the instrument was stopped to allow for data downloading and processing, the longest of which was 6 hours. Velocity was linearly interpolated at 10 min intervals to allow spectral analysis. The vertical shear was estimated from the ADCP data at 8 m depth bins:

$$S = dU/dz = \sqrt{\Delta u^2 + \Delta v^2}/8 \quad (2)$$

where u and v are the two components of the horizontal velocity and Δ indicates the difference between measurements in adjacent depth bins. The vertically averaged gradient Richardson number, Ri, the ratio of the stabilizing stratification to the destabilizing shear, was obtained from:

$$R_i = N^2/(dU/dz)^2 \quad (3)$$

The CTD data was initially subsampled at equivalent depth intervals to the ADCP data (8 m spacing) for the calculation of N^2, and the ADCP data subsampled at the same time intervals as each CTD cast, from which a median average was used to generate a profile of Ri versus depth. All data are described by reference to the time elapsed after the release, 1200 UTC on 9 February 1999.

3. Results

[11] The dispersion of the SF_6 patch during SOIREE is shown in Figure 1b, with the patch transported initially east and then southeast over a total distance of ~80 km during the 13 day experiment. Contour plots of the surface SF_6 did not indicate any distortion, bifurcation or appearance of secondary SF_6 maxima that would precede disintegration of the patch. Consequently, the SF_6 patch remained coherent with a defined central maximum throughout the experiment (see Figure 1b), as also confirmed by surface dissolved Fe distribution [*Bowie et al.*, 2001, Figure 5] and pCO_2 [*Bakker et al.*, 2001, Figure 2]. The patch expanded relatively rapidly in the first 24–48 hours from the initial release area of 50 km^2 to ~150 km^2, as the gradient at the patch boundary eroded and the SF_6 redistributed into an approximately normal distribution. Spreading subsequently decreased and the predominance of strain in determining dispersion resulted in a daily surface area increase of 7–8% from day 4 onward [*Abraham et al.*, 2000], as the patch elongated along its southeasterly transit axis. The dispersal of the SF_6 has been described by *Abraham et al.* [2000], with an estimated horizontal diffusivity, K_h, of 4 ± 2 $m^2 s^{-1}$ that is low compared with estimates of K_h from other SF_6 releases [*Martin et al.*, 2001], but within predicted estimates from dye releases in continental shelf regions [*Okubo*, 1971].

[12] The relatively slow lateral advection of the patch and its coherence assisted the determination of the patch bound-

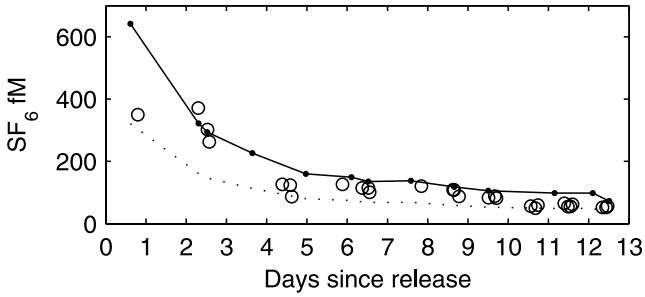

Figure 2. Comparison of surface SF_6 concentration (fmol/L) in the IN station profiles (open circles), with the maximum SF_6 concentration (fmol/L) recorded during underway surface analysis in the previous 6 hour period (line). The dotted line indicates 50% of the maximum underway surface SF_6.

ary and centre positions. Comparison of the surface SF_6 concentrations from the vertical hydrocasts with the underway data confirmed that SF_6 concentration at each IN station was >55% of the maximum concentration recorded in the previous 6 hours of mapping (Figure 2). During periods of high winds on day 2 ship drift was significant at the IN station, and necessitated correction of the ships position between hydrocasts by reference to the underway surface SF_6 signal. Surface SF_6 concentration declined throughout the experiment because of lateral mixing and air-sea exchange, from an initial maximum of approximately ~650 fmol/L (410 times background concentration) to a maximum of ~80 fmol/L (50 times background) on day 12. As concentrations remained significantly above background throughout the experiment further reinfusion with SF_6-saturated seawater was not required.

[13] There are no natural sources of SF_6 in the surface ocean, and the dissolved SF_6 at the OUT station originated from equilibration with the atmosphere. Mixed layer concentrations were relatively uniform and agreed with the predicted equilibrium concentration of 1.58 fmol/L (Figure 3), derived from a measured atmospheric mixing ratio of 3.9 pptv. SF_6 concentration remained relatively uniform to depths of ~120 m, indicating recent ventilation of subpycnocline water and inferring that this is the depth of deep winter mixing. At depths below 140 m there was a decline in SF_6 concentration, where recently ventilated water mixed with older water.

[14] The trends observed in the surface SF_6 mapping were reflected in the vertical profiles at the IN stations. The surface mixed layer was characterized by high SF_6 with a sharp gradient at the seasonal pycnocline between 60 and 70 m. The initial IN station profile displayed some variability in mixed layer SF_6 concentration (see Figure 4), although SF_6 was subsequently distributed uniformly in the surface mixed layer. Mixed layer SF_6 initially decreased rapidly as the patch spread and then stabilized at ~125 fmol/L after day 4, before decreasing again around day 10 to ~60 fmol/L where it remained constant to day 13. These two periods of stability in the surface SF_6 coincided with low to moderate wind speeds (see below). Agreement between SF_6 profiles within each station was good until day 11 when variability began to increase. This was attributed to the difficulty of maintaining the ship on the patch centre as the patch stretched in a NW-SE direction in response to mesoscale strain [*Abraham et al.*, 2000] and also to development of structure in the mixed layer. The depth profiles did not show immediate evidence of significant diapycnal transfer of SF_6, (see Figure 4), although this was partially obscured by vertical displacement of the pycnocline between 65 and 76 m by internal waves (see Figure 5). Variation in the structure and position of the pycnocline relative to the target isopycnal from which SF_6 was diffusing was not significant. As the dissolved SF_6 moves with density surface and not depth, the isopycnal displacement by internal waves was corrected for by initially referencing each SF_6 sample to the average density-depth profile using its respective density value [*Law et al.*, 1998]. This normalization to an average depth profile for the entire experiment facilitated comparison of SF_6 profiles.

[15] Wind speeds were low during the SF_6/iron release on day 0, but increased immediately afterward and remained above 12 ms^{-1} until day 4 (Figure 5a). The wind subsequently decreased to ~5 ms^{-1}, before increasing again to 12 ms^{-1} on day 9, and then subsiding to ~5 ms^{-1} for the remainder of the experiment. The stability, N^2, was initially uniform in the mixed layer, with maximal values of 5×10^{-3} s^{-2} in the seasonal pycnocline between 60 and 75 m (see Figure 5b). N^2 increased markedly at shallower depths in the mixed layer from $\sim 1 \times 10^{-6}$ s^{-2} before day 5 to $>1 \times 10^{-5}$ s^{-2} by the end of the experiment, reflecting the formation of transient structure in response to improved meteorological conditions and warming of surface waters [*Boyd et al.*, 2000]. The stratification at ~20 m on days 6–8 was weakened by an increase in vertical mixing in response to increased wind speed on day 9. Structure again became apparent at 20 m and also at 50 m between days 10–12 coincident with a further period of low wind speed (Figures 5a and 5b), which contributed to the variability between SF_6 profiles within stations on days 11 and 12. Overall the stability associated with this stratification resulted

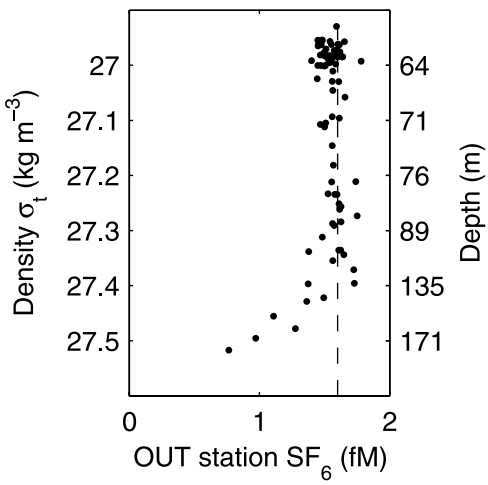

Figure 3. All OUT station SF_6 concentration data (fmol/L) plotted against density and nominal depth (derived from the average density-depth relationship), with the expected concentration from equilibrium with atmospheric SF_6 indicated by the dashed line.

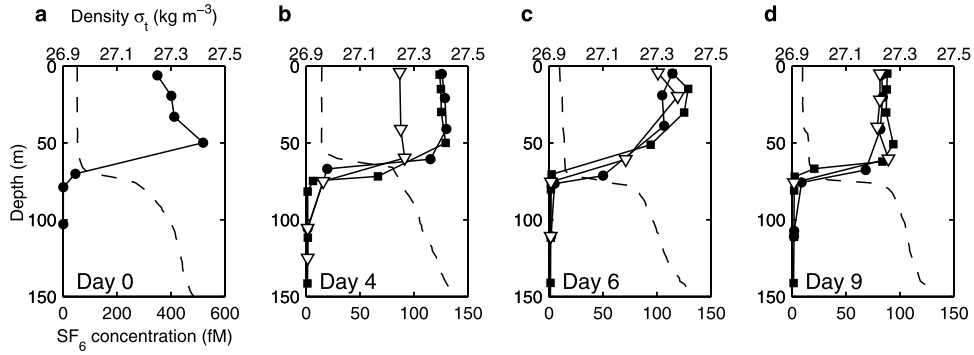

Figure 4. IN station SF_6 concentration (fmol/L) (solid lines) and density profiles (dashed lines) for (a) day 0, (b) day 4, (c) day 6, and (d) day 9. Only one profile was obtained on day 0, whereas three SF_6 profiles were obtained at the other IN stations.

in an N that was still one order of magnitude lower than within the seasonal pycnocline. Consequently, although mixing within the surface layer would have been influenced by the transient stratification, the seasonal pycnocline still represented the primary barrier to vertical diffusion of the SF_6.

[16] Shear was generally highest at the base of the surface mixed layer at 60 m, and remained relatively constant from 30–50 m throughout the experiment, except during the high winds on days 1–2 when it exceeded 10^{-2} s^{-1} in the pycnocline. Shear decreased toward the end of the experiment as wind speeds fell and stratification developed within the surface layer. All profiles showed a higher Ri and so greater dynamic stability in the seasonal pycnocline than within the surface layer, as expected. The Richardson number was not available for day 0–1, but exhibited lowest values at the base of the surface mixed layer on day 2 (see Figure 5d). This may reflect a relatively short temporal response to increased wind stress, as reported from microstructure measurements in shelf regions [*Oakey and Elliot*, 1982]. The development of stratification within the surface layer during the second half of the experiment caused an increase in Ri. Interestingly, Ri also increased markedly below the pycnocline to 120 m during this period, reflecting an increase in stratification.

[17] The total SF_6 in the patch was estimated at daily intervals from the surface underway SF_6 data assuming a mixed layer depth of 60 m, by a kriging contouring approach [*Law et al.*, 1998], and a second approach of fitting a Gaussian ellipsoid to the data [*Abraham et al.*, 2000, equation (1)]. The two estimates only deviated when the patch boundaries were not fully constrained during periods of limited mapping (days 5 and 10; see Figure 6), but otherwise showed good agreement. Air-sea exchange was the primary sink for SF_6, with high winds at the start of the experiment resulting in significant loss of tracer. This loss was potentially exacerbated by the high SF_6 gradient at the air-sea interface at this time, before the tracer had initially mixed into the surface layer. However, this was not significant, as 0.86 mol of the 1.1 mol SF_6 release was accounted for in the first mapping of the patch. Two estimates of SF_6 emission were obtained using the ship wind speed data and transfer velocity/wind speed parameterizations of *Wanninkhof* [1992] and *Nightingale et al.* [2000]. These confirmed that 30–35% of the tracer was lost to the atmosphere during the initial 4 days, compared with a subsequent loss of a further 10–12% on days 5–12. The good fit of the predicted estimates of air-sea loss to the observed data (see Figure 6) provides strong evidence that the patch was successfully constrained by the mapping surveys.

4. Analysis

[18] In order to estimate the vertical flux of SF_6, a theoretical model for the diffusion of a tracer within the pycnocline is required. As a simple approximation, it is assumed that the horizontal diffusivity, K_h, is isotropic, with no spatial or temporal variation within the region of interest over the duration of the experiment. In addition, air-sea exchange is ignored. The vertical diffusivity, K_z, is first considered to be a function of depth only, and the advection-diffusion equation for the dispersal of a tracer concentration C (x, y, z, t) (where x and y are horizontal directions, z is depth and t is time) may then be written

$$\frac{\partial C}{\partial t} + u\frac{\partial C}{\partial x} + v\frac{\partial C}{\partial y} + w\frac{\partial C}{\partial z} = K_h\left(\frac{\partial^2 C}{\partial x^2} + \frac{\partial^2 C}{\partial y^2}\right) + \frac{\partial}{\partial z}\left(K_z\frac{\partial C}{\partial z}\right) \tag{4}$$

where u, v and w are the advection velocities in the x, y, and z directions respectively. In previous tracer experiments [*Ledwell et al.*, 1986, 1998], both the vertical velocity w and the spatial variation of the vertical diffusivity, $\partial K_z/\partial z$, were estimated. However, the vertical sampling of the SF_6 distribution was not sufficiently resolved during SOIREE to warrant this approach, and so it was assumed that $w = 0$ and that the vertical diffusivity was a constant, $\partial K_z/\partial z = 0$, through the depth range of interest. If the horizontal velocities u and v are also independent of depth then equation (4) is separable, namely the concentration $C(x, y, z, t)$ may be written in terms of functions $f_h(x, y, t)$ and $C_z(z, t)$ as $C = f_h C_z$, provided that the initial condition also has this property. The development of the depth-dependent function, C_z, is then governed by the diffusion equation:

$$\frac{\partial C_z}{\partial t} = K_z\frac{\partial^2 C_z}{\partial z^2} \tag{5}$$

If $C_z(z, t)$ is the SF_6 concentration as a function of depth and time, C_∞ is the background concentration, C_0 is the

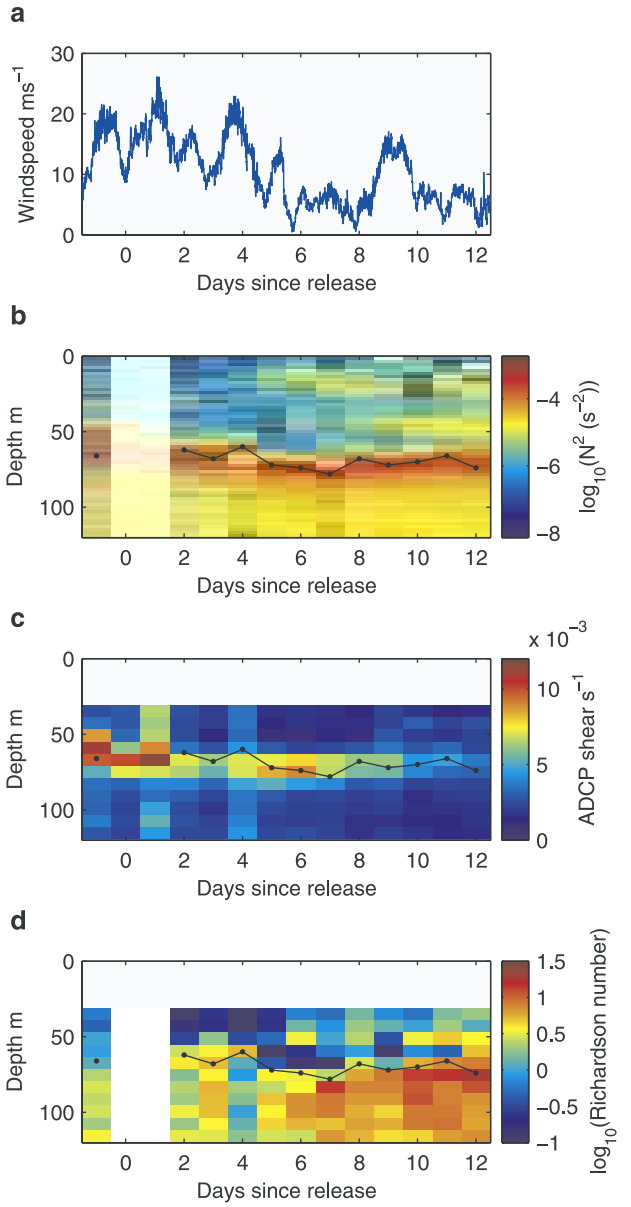

Figure 5. (a) Hourly wind speed (m s^{-1}), (b) daily averaged Brunt-Väisälä frequency, N^2 (s^{-2}), at 2 m depth bin intervals, (c) daily averaged vertical shear (s^{-1}) using all ADCP data, and (d) Richardson number *Ri* derived from data in Figures 5b and 5c as described in the text. The connected dots indicate the base of the surface mixed layer on each day, as determined from the maximum Brunt-Väisälä frequency, for comparison between plots. The upper depth bin for the ADCP was 31 m.

concentration within the mixed layer (assumed to be constant after $t = 0$), the mixed layer depth is z_m with a diffusivity of K_z below this depth, and the initial concentration $C_z(z, 0)$ is zero for depths $z > z_m$, then the solution to the diffusion equation (5) is

$$\frac{C_z(z,t) - C_\infty}{C_0 - C_\infty} = \begin{cases} 1 & (z \le z_m) \\ \mathrm{erfc}\left(\dfrac{z - z_m}{\sigma}\right) & (z > z_m) \end{cases} \quad (6)$$

where erfc is the complementary error function:

$$\mathrm{erfc}(x) = 1 - \frac{2}{\sqrt{\pi}} \int_0^x e^{-\beta^2} d\beta \quad (7)$$

and the width, σ, has the time dependence:

$$\sigma = 2\sqrt{K_z t} \quad (8)$$

A new approach was to fit complementary error functions to the data, and estimate the diffusivity from the increase in the width of the fitted functions, following equation (8). The complementary error function solution, equation (6), was fitted to the density-corrected SF_6 data from each station using a nonlinear least squares procedure. The background SF_6 concentration, C_∞, was taken to be 1.6 fmol/L (see Figure 3), and for each station the mixed layer SF_6 concentration, C_0, was set as equal to the mean of all measurements at depths <50 m. The scale, σ, was determined by minimizing the square of the difference between log ($C(z, t)$) and the logarithm of the measured SF_6 concentration. The logarithms were used as this reduced the dependence of the magnitude of the differences on the concentration. By repeating the fitting procedure for a range of mixed layer depths, it was found that the total least squares error from all the stations was minimized by z_m = 61.5 m. With this mixed layer depth, the fit of equation (6) generally showed good agreement with the average SF_6 density-corrected depth profiles for each station (Figure 7). The only significant deviation was on day 11, with the scatter in the data probably resulting from the combined influences of the development of thermal structure in the mixed layer, shear and the stretching of the patch [*Abraham et al.*, 2000]. Using a linear fit to the square of the scale, a K_z of 0.1 × 10^{-4} m^{2}s^{-1} was obtained from equation (8), with a 90% c.i. of −0.1 to 0.3 × 10^{-4} m^{2}s^{-1} (see Figure 8a).

[19] The complementary error function approach was compared to a method of estimating vertical diffusivity by calculating the second moments of the data [*Law et al.*, 1998, 2001]. The second moment, M_2, of the SF_6 concentration within the pycnocline is defined as

$$M_2 = \int_{z_m}^{\infty} (C(z) - C_\infty)(z - z_m)^2 dz \Big/ \int_{z_m}^{\infty} (C(z) - C_\infty) dz \quad (9)$$

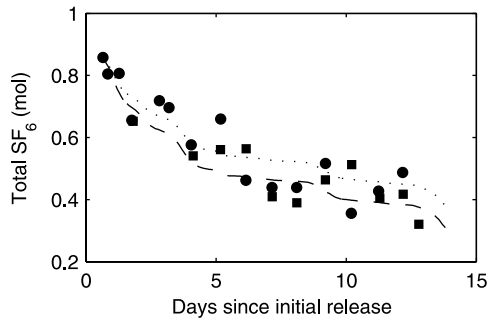

Figure 6. Total SF_6 (mol) in the SOIREE patch estimated from the surface underway data using integral (circles) and Gaussian fits (squares). Comparative predicted estimates based upon loss to the atmosphere are included using parameterizations of *Wanninkhof* [1992] (dashed line) and *Nightingale et al.* [2000] (dotted line).

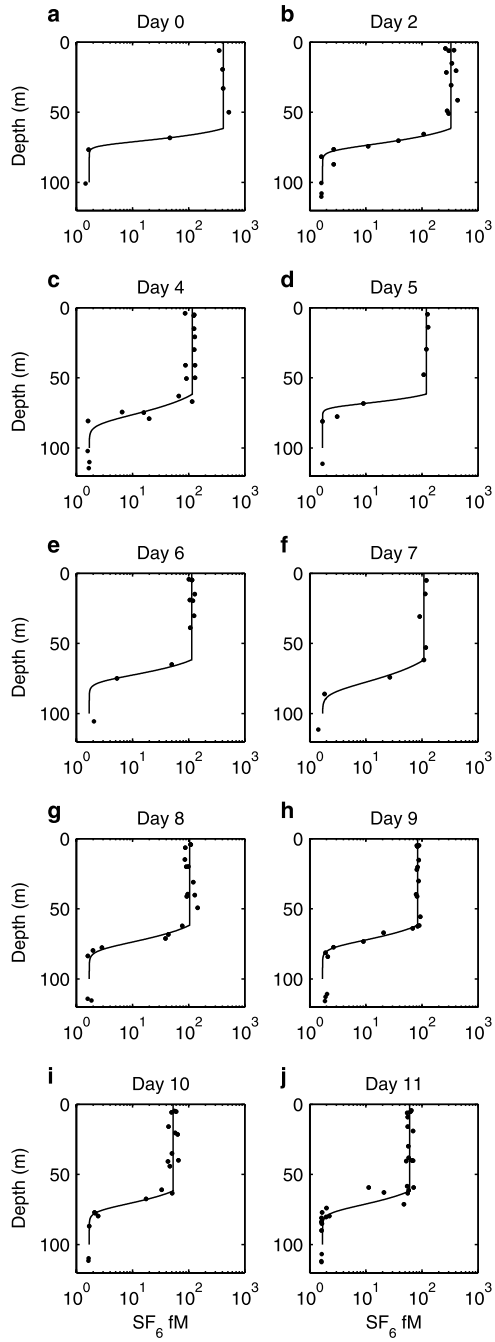

Figure 7. Complementary error function fits to the logged SF_6 concentration data (dots) for each station, the curves of which are given by equation (6).

For the complementary error function solution (6) the second moment is $M_2 = \sigma^2/3$, obtained using the integrals $\int_0^\infty \mathrm{erfc}(x)dx = 1/\sqrt{\pi}$ and $\int_0^\infty \mathrm{erfc}(x)x^2dx = 1/3\sqrt{\pi}$. The diffusivity may then be estimated from

$$K_z = 3/4\ dM_2/dt \tag{10}$$

Previous studies have used the second-moment equation appropriate to a Gaussian (or a half-Gaussian) to analyze surface SF_6 releases, in which $K_z = 1/2dM_2/dt$. This approach has been applied in analysis of point releases at depth [*Ledwell et al.*, 1986, 1993], but is less appropriate in describing diffusion across the seasonal pycnocline. For consistency with equation (10), the *Kz* values derived in previous surface SF_6 release studies [*Law et al.*, 2001; *Carse*, 2000] should be multiplied by a factor of 1.5.

[20] To estimate the second moment of the data, a mean SF_6 depth profile was generated from the data for each station (see Figure 4) to provide sufficient data points in the seasonal pycnocline. The density-corrected SF_6 depth profiles were linearly interpolated to 2.5 m intervals, with subtraction of the density-corrected background SF_6 profile, and the interpolated profiles for each station averaged together. Integration of the mean profiles gave a near daily estimate for the second moment, with the mixed layer depth assumed to be a constant 61.5 m. Linear regression was used to estimate the rate of increase of the second moment (see Figure 8b), with a diffusivity of $K_z = 0.2 \times 10^{-4}$ m^2s^{-1} obtained from equation (10), the 90% confidence interval (c.i.) on this estimate being -0.05 to 0.4×10^{-4} m^2s^{-1}.

[21] The large uncertainty in both estimates arises in part from limited sampling resolution in the pycnocline. However, spatial and temporal variation in the processes that determine diffusion also contribute. As vertical diffusion in the surface ocean varies temporally, with long periods of low activity punctuated by short intermittent bursts of enhanced diffusion [*Gregg*, 1987], the diapycnal dispersion of a tracer will not be linear with time, and this will introduce uncertainty in a time-integrated estimate of *Kz*, even when the spatial distribution is well resolved. While the two methods are based on the same theoretical model, they use a different analysis of the data. However, the two estimates of K_z agree within the confidence limits, confirming that vertical diffusivity at the base of the mixed layer was low, being less than 0.3×10^{-4} m^2s^{-1}. The fitting of complementary error functions is considered to be more reliable, as it does not require linear interpolation of the SF_6 data and is not subject to bias in the tail of the tracer decline, as with the second-moment approach. Consequently we take $K_z = 0.1\ (\pm 0.2) \times 10^{-4}$ m^2s^{-1} as the mean effective vertical diffusion for comparison with other estimates and calculation of diapycnal nutrient fluxes.

[22] Because the two methods are only sensitive to the shape of the SF_6 profiles, the separation of variables in equation (4) means that they will not be affected by changes in concentration caused by horizontal dispersal. There are three other approximations that are not accurate, namely that there was no vertical shear in the horizontal currents, that there was no air-sea loss of SF_6, and that there was no vertical variation of the vertical diffusivity. Air-sea exchange was significant, and would cause the profiles below the mixed layer to deviate from a precise complementary error function form. There was some evidence for the lateral injection of water from outside the patch below 50 m in both vertical SF_6 and dissolved inorganic carbon profiles on day 11 and 12 [*Bakker et al.*, 2001]. There was also further indication of shear distortion in the biological response to the iron addition at the end of the experiment, with chlorophyll fluorescence and the quantum photosynthetic efficiency, Fv/Fm, exhibiting variability in the surface mixed layer on the final patch transect [*Boyd et al.*, 2000; *Boyd and Abraham*, 2001]. If this reflected hydrodynamic

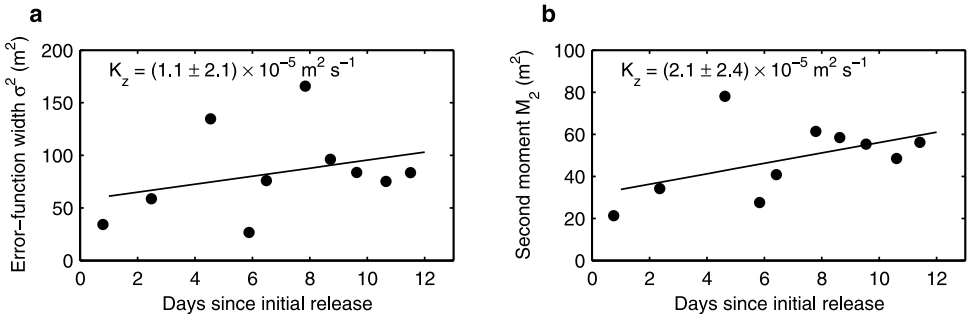

Figure 8. (a). Estimate of K_z from the increase in σ with time obtained by fitting complementary error functions (equation (8)). The errors on the quoted diffusivities are 90% confidence intervals. (b) Estimate of K_z from the increase in M_2 with time using an integral approach (equation (10)).

control of the biology, as opposed to a biotic response to iron or light availability, then the inferred decoupling of the base of the surface layer from the overlying surface water could result in underestimation of K_z.

[23] A numerical model of the three-dimensional dispersal of SF_6 in the pycnocline was developed to examine the effectiveness of the error function method, and determine whether inclusion of processes, such as air-sea exchange and vertical shear in the horizontal currents, in the analysis would significantly alter the calculated K_z. The ADCP data and an assumed vertical diffusivity were used to simulate the dispersal. The numerical domain was a three-dimensional grid of 24 layers, each separated by 0.5 m, with horizontal dimensions of 121 × 61 grid points at intervals of 500 m. The SF_6 concentration in the upper layer was determined from the analytically calculated dispersal of a tracer in a pure strain flow [*Abraham et al.*, 2000]. The horizontal velocities were $u = \gamma x$ and $v = -\gamma y$, with values for the strain ($\gamma = 8 \times 10^{-7}$ s^{-1}) and horizontal diffusivity ($K_h = 4$ $m^2 s^{-1}$) determined from analysis of the horizontal spread of the SF_6 patch [*Abraham et al.*, 2000]. The surface concentration was also allowed to decline to simulate the loss of SF_6 to the atmosphere, using the *Nightingale et al.* [2000] parameterization. The upper model layer was assumed to be at a depth of 61 m, and the calculated concentration gave a good representation of the surface layer SF_6 data. A one-dimensional Crank-Nicholson diffusion scheme, with a nominal vertical diffusivity of 0.2×10^{-4} $m^2 s^{-1}$, was applied at time steps of one hour to each vertical column to mix the modeled SF_6 between layers. At each time step, the linearly interpolated ADCP currents were also used to advect the concentration within each layer. A cross section through the pycnocline of the modeled patch is shown in Figure 9, after an integration time of 12 days. Shear within the region immediately beneath the base of the surface layer was not significant enough to destroy the vertical coherence of the patch. The maximum SF_6 is not at the base of the mixed layer but ~2 m below, as a result of SF_6 loss to the atmosphere.

[24] In addition to accounting for the influence of shear on the SF_6 distribution, the model data set was also used to check whether the complementary error function method was appropriate to the analysis of the profile data. By taking a vertical profile from the modeled patch once per day, with the position of the profile chosen randomly in the area where the mixed layer SF_6 concentration exceeded 50% of the peak concentration, a simulated set of profiles was obtained. Calculating second moments of the concentration gave $K_z = 0.23 \pm 0.06 \times 10^{-4}$ $m^2 s^{-1}$ (90% c.i.) from equation (10), whereas fitting complementary error functions to these profiles gave an estimate of $K_z = 0.16 \pm 0.05 \times 10^{-4}$ $m^2 s^{-1}$ (90% c.i.) from equation (8). The fitting procedure was carried out so that both the scale and the mixed layer depth in equation (6) were determined by a minimization procedure, applied to each profile independently. The uncertainty (estimated by repeating the sampling and fitting procedures 500 times) represents the expected error of any one experimental determination of the diffusivity; the error in the mean is over an order of magnitude smaller. The complementary error function approximation results in an underestimate of K_z on the order of 20%, while the second-moment approach overestimates by a similar percentage. Although the omission of air-sea loss and vertical shear in the horizontal currents results in some bias, this is small relative to other errors in the estimation of the diffusivity.

[25] A further potential factor that may have obscured SF_6 penetration across the pycnocline is an increase in vertical diffusion in subpycnocline waters. SF_6 diffusing from the surface mixed layer would not accumulate if the water column beneath the pycnocline was unstable, leading to an underestimation of K_z. This was examined with reference to the gradient Richardson number, which provided an indication of stability in the subpycnocline region. It is clear from Figure 10 that the stability of the water column increased with depth below the mixed layer, and so

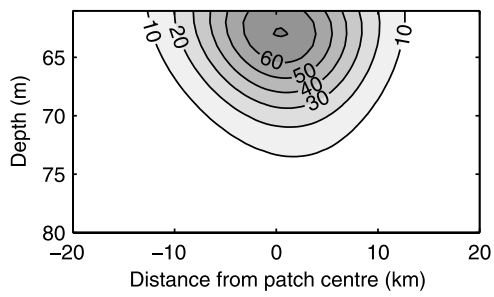

Figure 9. Section through the base of the mixed layer showing SF_6 concentration (fmol/L) distribution on day 12, as predicted from the three-dimensional dispersal model.

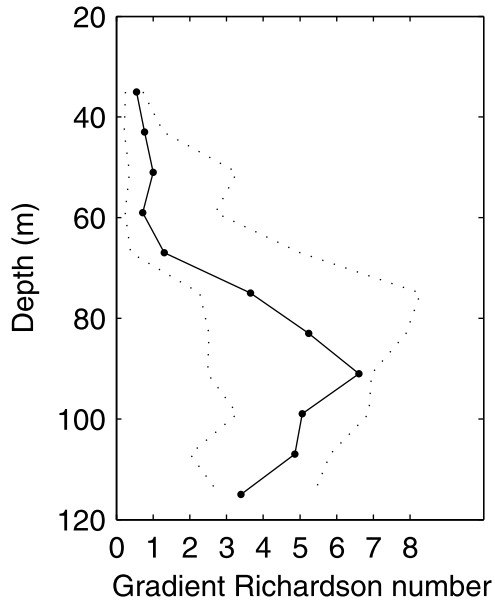

Figure 10. The median gradient Richardson number depth profile (solid line) with the upper and lower quartiles shown as dotted lines. The daily averaged data shown in Figure 5 is used to generate the profiles.

vertical diffusivity is unlikely to have increased in or below the pycnocline.

5. Discussion

5.1. Control of Vertical Eddy Diffusion at the Base of the Surface Mixed Layer

[26] Although there is no evidence confirming the source of the energy for vertical diffusion, there is some indication of the role of both wind stress and stratification in influencing K_z. The internal wave field was influenced by the passage of atmospheric low-pressure systems, and strong vertical velocity shear generated by high winds. The dominance of high winds in the first few days of the experiment, followed by calmer conditions for the remainder of the experiment influenced the stability and shear in the surface mixed layer (see Figure 5). Vertical diffusion was potentially elevated during the first 3–4 days of the experiment in response to high winds and shear at the base of the mixed layer. If we assume an initial width equal to zero at $t = 0$, a K_z of 0.8 ± 0.2 (90% C.I.) $\times 10^{-4}$ m^2s^{-1} was obtained for days 1–4 using the complementary error function approach. This is based on limited data and would require a $K_z \leq 0$ for the remainder of the experiment, although Figure 8 suggests that the error function widths do not increase significantly after day 4. Subsequently, light winds led to the development of structure in the surface mixed layer between days 5 and 8 (Figure 5b), providing a barrier to the vertical transfer of turbulent kinetic energy. It was not established whether this stratification was a permanent diel feature, or whether it was eroded by nighttime convection. The formation of further stratification at 20 and 50 m from day 10 onward coincided with a reduction in shear at the base of the mixed layer (see Figure 5c), and little change in the width of the error functions (see Figure 8a).

[27] Despite the large uncertainty, the two estimates confirm an upper limit on K_z of 0.3×10^{-4} m^2s^{-1} in agreement with previous estimates [*Broecker*, 1981] indicating that vertical diffusion across the seasonal pycnocline in this region is low. The calculated mean effective K_z of $0.1 \pm 0.2 \times 10^{-4}$ m^2s^{-1} from the complementary error function fits is lower than that reported for other regions [*Law et al.*, 1998, 2001; *Carse*, 2000], though comparable with microstructure estimates in the seasonal pycnocline of the equatorial Pacific [*Carr et al.*, 1992] and in the deep ocean [*Polzin et al.*, 1995, 1997]. A low diapycnal exchange rate is surprising when considered in the context of the dynamic meteorological conditions that characterize the ACC, where wind speeds represent global maxima. However, this assumes a direct relationship, whereas a correlation between wind speed and current shear at the base of the mixed layer was only apparent during high winds on days 1–2 (see Figures 5a and 5c). Wind stress may have more influence upon cross-pycnocline exchange via the initiation and maintenance of inertial oscillations and associated current shear. Lateral dispersion of the tracer was influenced by inertial oscillations during the initial part of the experiment [*Abraham et al.*, 2000], with spectral analysis of the ADCP current velocity data showing a large peak between 13.2 and 14.3 hours, in agreement with the inertial period of $12/\sin(61°) = 13.72$ hours. The energy associated with this declined sharply below 50 m, indicating that shear at the pycnocline was driven by the inertial oscillation (Figure 11a). The amplitude of the inertial oscillations exhibited a maximum at day 1, with a decline throughout the experiment. Figure 11b shows that the majority of the current shear was generated at the inertial frequency, whereas little was derived from high and low frequencies, confirming that vertical diffusion across the pycnocline was predominately associated with the inertial oscillation.

[28] How representative is the SOIREE K_z of the ACC during the Austral summer? Hourly wind speeds during SOIREE (mean 9.3 ± 5 ms^{-1}) showed good agreement with wind speed data for each day at 61°S 140°E for 1991–2000 (9.25 ± 1.4 ms^{-1}) from ECMWF operational analysis (see Figure 12). Between days 1 and 5 the mean daily wind speed (13.2 ± 3.9 ms^{-1}) was significantly greater than the ECMWF average, and decreased by a factor of two for the remainder of the experiment (6.2 ± 3.2 ms^{-1}), although neither period represented extremes. This trend is consistent with the regular pattern of intense low-pressure systems at 3–4 day intervals that characterize this region of the Southern Ocean. Vertical diffusion at the base of the mixed layer in the ACC may then be dominated by periods of high winds and maintained by current shear associated with wind-driven inertial shear, declining during intervening periods when the dissipation of energy from the vertical propagation of surface forcing does not penetrate to the seasonal pycnocline. Whereas this may be speculative, the SOIREE took place during a typical pattern of weather conditions for this region, and so the K_z obtained is considered representative of the ACC during the Austral summer.

5.2. Parameterization of Diffusivity at the Base of the Mixed Layer

[29] A parameterization of K_z is required for realistic representation within numerical models of ocean circulation

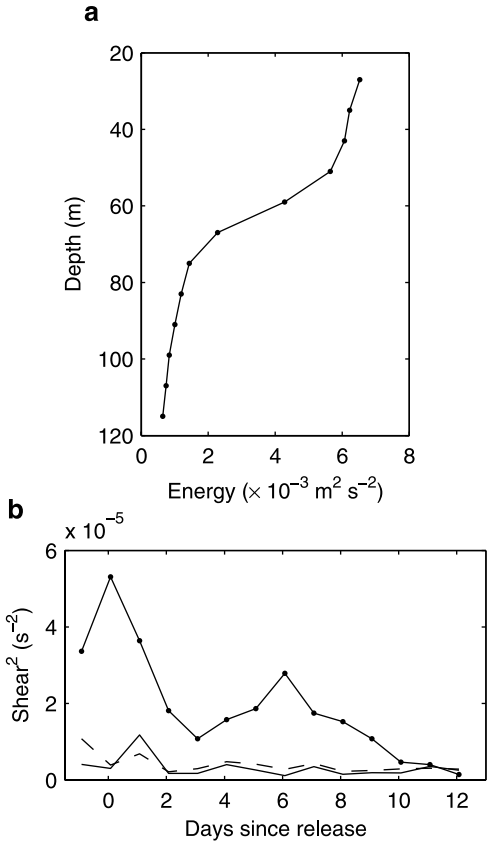

Figure 11. (a). Depth variation in the energy associated with the inertial oscillation. The figure shows the energy between 12.7 and 14.9 hours, obtained by integrating the cyclic periodogram of the *u* and the *v* components of the interpolated ADCP data from within each depth bin. (b) Variation in the shear at inertial frequency (solid line connecting dots), high frequency (dashed line), and low frequency (solid line) with time. The shear across the pycnocline is estimated from the difference between the interpolated ADCP velocities in the 59 m and the 67 m depth bins. The energy is estimated by integrating the cyclic periodograms of a moving 27.83 hour long subset of the shear data. The inertial frequency range spans the periods 11.1–18.6 hours, with the low-frequency band having periods higher than this range (including the mean) and the high-frequency band having periods shorter than this range.

and for predicting rates of turbulent supply in biogeochemical budgets and models. Development of a parameterization using a relatively accessible variable is preferable, such as wind speed in the case of air-sea exchange [*Wanninkhof*, 1992; *Nightingale et al.*, 2000]. However, whereas local wind stress influences the majority of processes that control air-sea exchange, the situation is not as simple at the base of the mixed layer because of the variable contributions of local and nonlocal forcing. Existing model parameterizations have often been chosen arbitrarily or adjusted to achieve agreement between density and velocity fields [*Gregg*, 1987]. There is good evidence to indicate that in the deep ocean, away from regions of boundary mixing and local sources of energy, K_z is primarily controlled by the internal wave field and so is inversely proportional to the buoyancy frequency N [*Gargett*, 1984; *Gregg*, 1987]. In highly stratified systems such as at the base of the surface mixed layer, compression of the isopycnals suppresses the development of turbulence and consequently N-based proportionality may also apply. This is supported by evidence from compilations of K_z in the open ocean, shelf regions and lakes, which indicate N-based dependence of K_z at the base of the surface mixed layer [*Quay et al.*, 1980; *Law et al.*, 2001]. However, the $K(N)$ relationship of *Law et al.* [2001] predicts a K_z of 2×10^{-4} $m^2 s^{-1}$ for SOIREE, which is an order of magnitude greater than that observed. Previous analysis of the Ironex1 and PRIME data was based on the assumption that the rate-limiting point for vertical diffusion across the seasonal pycnocline corresponded to the maximum N [*Law et al.*, 2001], whereas analysis of the SOIREE data set indicated that diapycnal diffusion of SF_6 was restricted by relatively minor increases in density and N. As a result, the data from Ironex1 and PRIME have been reassessed using the median N, consistent with the approach of *Strang and Fernando* [2001], at the midpoint depth of the SF_6 tracer decline. Inclusion of the revised data and the SOIREE K_z with other reported values shows a greater spread with no clear linear relationship between N and K_z (see Figure 13a). Whereas linear $K(N)$ relationships have been obtained within various systems [see *Quay et al.*, 1980] the apparent lack of a global $K(N)$ relationship in Figure 13a is perhaps not too surprising as the data were derived using different approaches in surface mixed layers of varying depth in tropical, temperate and polar waters.

[30] A further consideration is that an N-based parameterization takes no account of locally generated shear and associated dissipation. A more appropriate function for the parameterization of K_z may be the gradient Richardson number, Ri, which represents the balance between the

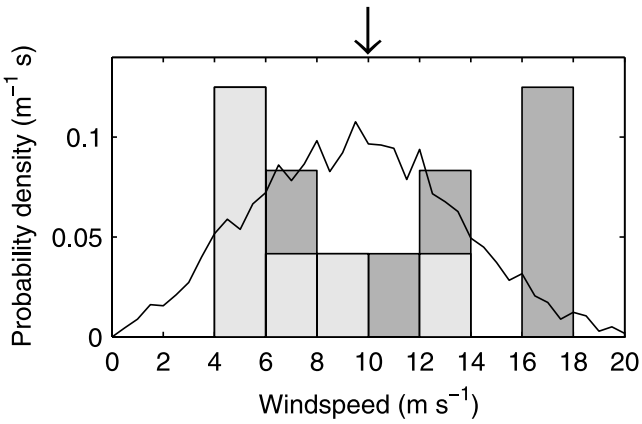

Figure 12. Frequency distribution of mean daily wind speeds over a 10 year period (1991–2000) at 61°S 140°E as predicted from ECMWF (solid line), normalized to form a probability density function (pdf). The average wind speed for each day is shown as a histogram, also normalized as a pdf, with the first 6 days of generally higher wind speed represented by the dark shading and the final 6 days of lower wind speed indicated by the lighter shading.

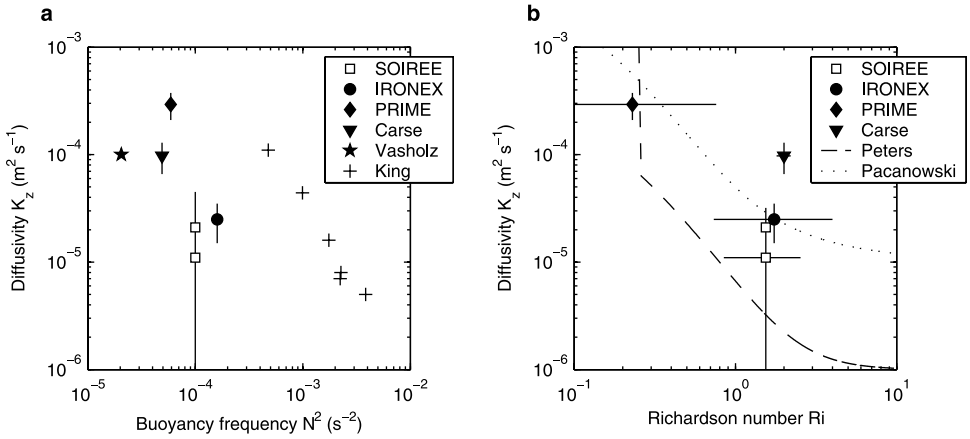

Figure 13. (a) Relationship between buoyancy frequency $\log_{10}$ (N) and diffusivity $\log_{10}$ (K_z), using estimates from tracer, dye, and nitrogen turnover experiments. (b) Relationship between $\log_{10}$ (Ri) and diffusivity $\log_{10}$ (K_z), using tracer-derived K_z estimates. Key: SOIREE, K_z derived from second-moment analysis and from fitting complementary error functions, plotted against median N and Ri in the upper pycnocline (this study); IRONEX, SF_6 tracer-derived K_z (second-moment approach) and median N and Ri from IronEx1 in the equatorial Pacific [*Law et al.*, 1998]; PRIME, SF_6 tracer-derived K_z (second-moment approach) and median N and Ri from the PRIME study in an anticyclonic eddy in the North Atlantic [*Law et al.*, 2001]; Carse, SF_6 tracer-derived K_z (second-moment approach) and maximum N and Ri from the ACSOE study in an anticyclonic eddy in the North Atlantic [*Carse*, 2000]; Vasholz, dye tracer-derived K_z and mean Ri on the Florida Shelf [*Vasholz and Crawford*, 1985], King, integrated nitrate uptake/supply estimate of K_z and N derived from σ_t gradient at base of mixed layer [*King and Devol*, 1979]; Peters, parameterization based on microstructure measurements of the Equatorial Undercurrent [*Peters et al.*, 1988]; and Pacanaowski, parameterization based on a model of microstructure data from the Equatorial Undercurrent [*Pacanaowski and Philander*, 1981]. The original second-moment estimates of K_z for PRIME and Carse have been revised for compatibility with equation (10).

stabilizing buoyancy frequency and the destabilizing shear. Functional relationships had been developed for $K(Ri)$, with the most extensive obtained in shear flow regions in the Equatorial Undercurrent [*Pacanowski and Philander*, 1981; *Peters et al.*, 1988]. These relationships indicate a monotonic increase in mixing from Ri of 10 to 0.3, with a sharp increase in diffusivity at $Ri < 0.3–0.4$ [*Peters et al.*, 1988] (see Figure 13b), coincident with the initiation of local shear instability and turbulent flow. Recently, *Strang and Fernando* [2001] used a laboratory stratified shear layer model to confirm that Ri describes the nature of the shear layer at the base of the mixed layer in the ocean, and so determines the mechanism of mixing. The tracer-derived K_z and associated Ri data show reasonable agreement with reported $K(Ri)$ parameterizations, with the uncertainty on the estimates encompassed by the $K(Ri)$ relationships of *Pacanowski and Philander* [1981] and *Peters et al.* [1988] (see Figure 13b). The *Peters et al.* [1988] parameterization for the Equatorial Undercurrent predicts lower values, although their hourly microstructure data show variation with higher K estimates at latitudes >1.5° consistent with the SOIREE tracer-derived estimates. The distribution of the data points in the plots of $K(Ri)$ and $K(N)$ show similar variability and so, based upon the limited data available, Ri does not appear to provide improved prediction of Kz. *Strang and Fernando* [2001] reported improved agreement between laboratory-based data and the $K(Ri)$ parameterizations of *Pacanowski and Philander* [1981] and *Peters et al.* [1988], when the length scale of the shear layer was considered. Consequently concurrent measurements of tracer distribution, microstructure turbulence and shear are required at increased resolution to fully constrain the relationship between K_z and Ri in the ocean.

5.3. Nutrient Exchange Across the Seasonal Pycnocline and Implications for Production

[31] Diapycnal nutrient supply to the surface mixed layer has been estimated using diffusion coefficients that are generated indirectly [*de Baar et al.*, 1995], from regional or local microstructure measurements [*Carr et al.*, 1992] and from tracer dispersion [*Law et al.*, 1998, 2001]. The vertical profiles at the OUT stations indicated that subpycnocline water was a potential source of nutrients [*Bowie et al.*, 2001], and concurrent determination of K_z and nutrient gradients provided a first direct estimate of diffusive supply across the seasonal pycnocline in the Southern Ocean. This was obtained by applying a diffusion coefficient to the interfacial gradient, in an extension of Fickian theory of molecular diffusion using the following equation:

$$\text{Flux} = K_z.(\Delta nut/\Delta z) \tag{11}$$

where Δnut represented the difference in nutrient concentration across the pycnocline over the depth range Δz (60–80 m) at the OUT and prerelease stations. The observed nitracline of 183 μmol m^{-4} would support a nitrate flux of 0.17 (upper c.i. 0.5) mmol $m^{-2}d^{-1}$ and supply 2.9 (upper c.i. 8.4) nmol $l^{-1}d^{-1}$ in a 60 m deep surface mixed layer. Assuming a C:N of 6.6, this would account for only 8% (24% maximum, using the upper c.i. on K_z) of the nitrate required to maintain carbon fixation rates at the OUT station (0.17 g C m^{-2}) [*Gall et al.*, 2001]. The mixed layer nitrate

concentration (~25 μmol/L) during SOIREE represented ~86% of that supplied by deep mixing during the previous winter [*Frew et al.*, 2001; *Trull et al.*, 2001], and so nitrate was clearly not limiting.

[32] Silicic acid ($Si(OH)_4$) in the surface mixed layer increased along the southerly transect to the SOIREE site, in line with reported meridional gradients across the ACC [*Daly et al.*, 2001; *Brzezinski et al.*, 2001; *Parslow et al.*, 2002]. Mixed layer silicic acid concentrations at the SOIREE site were intermediate at ~8–10 μM, and represented only 30–41% of that resulting from deep winter mixing [*Frew et al.*, 2001; *Trull et al.*, 2001]. An excess of nitrate relative to silicic acid is characteristic of circumpolar waters between the Polar Front and Sub Tropical Front [*Zentara and Kamykowski*, 1981; *Brzezinski et al.*, 2001]. This arises from preferential drawdown of silicic acid relative to nitrate in response to low iron availability [*Takeda*, 1998], although differential regeneration in subpycnocline waters may also contribute [*Dugdale et al.*, 1995]. Consequently the silicic acid gradient at the pycnocline (1.39 mmol m^{-4}) was steeper than that of nitrate, with a vertical diffusional supply of 1.32 (upper c.i. 3.84) mmol $m^{-2}d^{-1}$, or 22 (upper c.i. 64) nmol $l^{-1}d^{-1}$ integrated over a 60 m mixed layer. This is equivalent to 27% (75% maximum) of the phytoplanktonic requirement, as determined by ^{32}Si uptake incubations at the OUT station during SOIREE [*Watson et al.*, 2000]. The Si:N of the vertical diffusive supply was 7.5, in agreement with that reported for net seasonal drawdown in the Pacific ACC [*Sigmon et al.*, 2002] and for Si:N uptake ratios in iron-limited deck incubations [*Franck et al.*, 2000]. Whereas silicic acid did not limit diatom growth in this region, diapycnal supply will delay the southerly migration of the silicic acid front across the ACC during the Austral summer [*Brzezinski et al.*, 2001], extending the temporal window for diatom growth and export.

[33] Deep water represents the primary source of dissolved iron to the surface mixed layer of the Southern Ocean [*de Baar et al.*, 1995; *Löscher et al.*, 1997]. Deep mixing during winter elevates mixed layer iron concentration but this declines from spring onward in response to phytoplankton uptake and export until iron becomes limiting. Upwelling south of the Polar Front supplies 8–16 μmol $m^{-2}yr^{-1}$ [*Watson et al.*, 2000] and potentially 47 μmol $m^{-2}yr^{-1}$ [*de Baar et al.*, 1995], but this is predominately localized in regions of frontal activity. The absence of isopycnal erosion and the distance of the SOIREE site from frontal regions [*Trull et al.*, 2001] suggest that the contribution of upwelling in this region was not significant. Aeolian dust input represents another potential source of iron, although the Southern Ocean receives the lowest dust deposition per unit area in the world. Aeolian iron input to the Southern Ocean was considered to be on the order of 5–50 nmol $m^{-2}d^{-1}$ [*Duce and Tindale*, 1991], although uncertainties in the transition state and solubility of iron dust have subsequently led to lower revised estimates (2.7–27 nmol $m^{-2}d^{-1}$) [*Fung et al.*, 2000]. *De Baar et al.* [1995] calculated that aeolian iron input was similar in magnitude to the iron supply by vertical diffusion (based upon an inferred K_z of 0.3×10^{-4} m^2s^{-1}), with each pathway supplying 15 nmol Fe $m^{-2}d^{-1}$. More recently, *Bowie et al.* [2001] used revised estimates of iron dust solubility and an atmospheric model to obtain a dust supply of 0.27 nmol $m^{-2}d^{-1}$ to the SOIREE region, in agreement with estimates of 0.55 nmol $m^{-2}d^{-1}$ [*Lefevre and Watson*, 1999]. The dissolved iron gradient in the seasonal pycnocline (50–80 m), of 3 nmol m^{-4}, at the SOIREE OUT stations [*Bowie et al.*, 2001] inferred a vertical diffusive supply of 3 nmol $m^{-2}d^{-1}$ (upper bound 8.3 nmol $m^{-2}d^{-1}$). Consequently, although the mean effective K_z calculated for SOIREE is lower than previously considered, diapycnal diffusion may still supply an order of magnitude more iron than dust deposition. Vertical turbulent supply is therefore an important component of the iron budget in regions of the Southern ocean that do not experience frontal activity and upwelling.

[34] The contribution of vertical eddy diffusion to the phytoplanktonic iron requirement is highly dependent upon the Fe:C ratio. *Maldonado et al.* [2001] report an average of 2.73 ± 1.38 μmol Fe mol C during SOIREE, consistent with reported values of 3 μmol Fe mol C for oceanic species [*Sunda and Huntsman*, 1995; *Maldonado and Price*, 1996]. However, a Fe:C ratio of <1 μmol Fe mol C was measured during the latter part of the SOIREE when the population was exhibiting iron stress [*Maldonado et al.*, 2001]. As no differences were observed between the Fe:C uptake at the IN and OUT stations, this ratio is considered representative of background (e.g., iron-deplete) conditions. Application of this ratio suggests that vertical eddy diffusion could supply 20% (upper bound 58.5%) of the total phytoplanktonic iron requirement in the SOIREE region. However, recycling of iron in HNLC waters such as the Southern ocean is relatively high [*Maldonado et al.*, 2001], with iron regeneration rates during SOIREE of ~73–91% [*Bowie et al.*, 2001], consistent with the 76–95% iron regeneration predicted by the model of *Fung et al.* [2000]. Comparison of the calculated diffusive supply of dissolved iron with that regenerated then suggests that the new iron requirement in the SOIREE region of the ACC could potentially be almost entirely supplied by diffusion across the seasonal pycnocline. It should be noted that this estimate was obtained using the most conservative estimate of K_z from the complimentary error functions fit. These observations suggest that the diffusive supply of iron may provide a first approximation of carbon export in regions of the ACC that do not experience upwelling, and that establishing vertical supply is then critical for a full evaluation of the sources of iron in the ocean. Furthermore, the inverse relationship between K_z and N suggests that climate-induced warming of the surface ocean and associated increases in stratification may reduce the diffusive iron supply, with implications for production and export [*Boyd*, 2002].

[35] The supply of iron across the seasonal pycnocline may partially explain the paradox of the deep chlorophyll maximum (DCM) in Southern ocean waters. A DCM is a characteristic feature of ACC and sub-Antarctic waters, though one that defies an immediate explanation [*Parslow et al.*, 2002]. The apparent maintenance of a viable phytoplankton population in the DCM has been attributed to various factors including sinking, subduction and physiological adaptation [*Cullen*, 1982; *Parslow et al.*, 2002]. One explanation is that phytoplankton proliferate at the top of the nutricline, where nutrients are accessible in an otherwise nutrient-limited surface mixed layer. In iron-limited regions of the ACC phytoplankton in the DCM then have an advantage in accessing the diffusive supply of dissolved

iron before it is diluted into the surface layer, although this supply must be sufficient to overcome the elevated iron requirement under low-light conditions [*Sunda and Huntsman*, 1997]. Evidence for this has been reported for 54°S, where the Si:N uptake ratio in the DCM was low consistent with iron-replete conditions, despite a low mixed layer iron concentration [*Parslow et al.*, 2002]. The results presented here suggest that the DCM in ACC waters, which was observed along 139°E prior to SOIREE [*Trull et al.*, 2001], may be sustained by the diffusive supply of dissolved iron across the seasonal pycnocline.

[36] **Acknowledgments.** We acknowledge the help of Greg Jameson for development of the control system, Roger Ling for technical assistance, Ken Downing for CTD operation, Matt Walkington for the final data, Stuart Pickmere for the nutrient data, and Dorothee Bakker for organization and planning. Many thanks to the scientific cruise leaders Philip Boyd and Rob Murdoch, the Captain, Officers and Crew of the R/V *Tangaroa*, and all the SOIREE team for their help and assistance. We also thank Adrian Martin and Tim Stanton for locating and reanalyzing the PRIME and Ironex1 data sets. The data from the ECMWF (European Centre for Medium range Weather Forecasts) operational analysis was supplied by the British Atmospheric Data Centre (BADC) with access and manipulation by Tim Smyth. We also thank Philip Boyd and Craig Stevens for constructive comments. This study was partly funded by the UK Natural Environment Research Council through the Plymouth Marine Laboratory core strategic research program Microbially Driven Biogeochemical Cycles (MDB), and is MDB contribution number 39. This study was also supported by a UK Natural Environment Research Council Grant Award (No. GR3/A1431) and the NZ PGSF Fund for Antarctic Research.

References

Abraham, E. R., C. S. Law, P. W. Boyd, S. J. Lavender, M. Maldonado, and A. R. Bowie, Importance of stirring in the development of an iron-fertilised phytoplankton bloom, *Nature*, *407*, 727–730, 2000.

Bakker, D. C. E., A. J. Watson, and C. S. Law, Southern Ocean iron enrichment promotes inorganic carbon drawdown, *Deep Sea Res., Part II*, *48*, 2483–2508, 2001.

Bowie, A. R., M. T. Maldonado, R. C. Frew, P. L. Croot, E. P. Achterberg, R. F. C. Mantoura, P. J. Worsfold, C. S. Law, and P. W. Boyd, The fate of added iron during a mesoscale fertilisation experiment in the Polar Southern Ocean, *Deep Sea Res. Part II*, *48*, 2703–2744, 2001.

Boyd, P. W., Environmental factors controlling phytoplankton processes in the Southern Ocean, *J. Phycol.*, *38*, 844–861, 2002.

Boyd, P. W., and E. R. Abraham, Iron-mediated changes in phytoplankton photosynthetic competence during SOIREE, *Deep Sea Res., Part II*, *48*, 2529–2550, 2001.

Boyd, P. W., and C. S. Law, The Southern Ocean Iron Enrichment Experiment (SOIREE)—Introduction and overview, *Deep Sea Res., Part II*, *48*, 2425–2438, 2001.

Boyd, P. W., et al., Phytoplankton bloom upon mesoscale iron fertilisation of polar Southern Ocean waters, *Nature*, *407*, 695–702, 2000.

Broecker, W. S., Geochemical tracers and ocean circulation, in *Evolution of Physical Oceanography*, edited by B. A. Warren and C. A. Wunsch, pp. 434–461, MIT Press, Cambridge, Mass., 1981.

Bryan, F., Parameter sensitivity of primitive equation ocean general circulation models, *J. Phys. Oceanogr.*, *17*, 970–985, 1987.

Brzezinski, M. A., D. M. Nelson, V. M. Franck, and D. E. Sigmon, Silicon dynamics within an intense open-ocean diatom bloom in the Pacific sector of the Southern Ocean, *Deep Sea Res., Part II*, *48*, 3997–4018, 2001.

Carr, M.-E., N. S. Oakey, B. Jones, and M. R. Lewis, Hydrographic patterns and vertical mixing in the equatorial Pacific along 150°W, *J. Geophys. Res.*, *91*, 611–626, 1992.

Carse, F., Lake and ocean vertical mixing using sulphur hexafluoride tracer techniques, Ph.D thesis, 214 pp., Univ. of East Anglia, Norwich, UK, 2000.

Cullen, J. J., The deep chlorophyll maximum: Comparing vertical profiles of chlorophyll *a*, *Can. J. Fish. Aquat. Sci.*, *39*, 791–803, 1982.

Daly, K. L., W. O. Smith Jr., G. C. Johnson, G. R. DiTullio, D. R. Jones, C. W. Mordy, R. A. Feely, D. A. Hansell, and Z.-Z. Zhang, Hydrography, nutrients and carbon pools in the Pacific sector of the Southern Ocean: Implications for carbon flux, *J. Geophys. Res.*, *106*, 7107–7124, 2001.

de Baar, H. J. W., and P. W. Boyd, The role of plankton ecology and carbon dioxide transfer of the global oceans, in *The Dynamic Ocean Carbon Cycle: A Midterm Synthesis of the Joint Global Ocean Flux Study*, edited by H. W. Ducklow, J. G. Field, and R. B. Hanson, pp. 61–140, Cambridge Univ. Press, New York, 2000.

de Baar, H. J. W., J. T. M. de Jong, D. C. E. Bakker, B. M. Loscher, C. Veth, C. Bathmann, and V. Smetacek, Importance of iron for plankton blooms and carbon dioxide drawdown in the Southern Ocean, *Nature*, *37*, 412–415, 1995.

Duce, R. A., and N. W. Tindale, Atmospheric transport of iron and its deposition in the ocean, *Limnol. Oceanogr.*, *36*, 1715–1726, 1991.

Dugdale, R. C., F. P. Wilkerson, and H. J. Minas, The role of the silicate pump in driving new production, *Deep Sea Res., Part I*, *42*, 697–719, 1995.

Franck, V. M., M. A. Brzezinski, K. H. Coale, and D. M. Nelson, Iron and silicic acid concentrations regulate Si uptake north and south of the Polar Frontal Zone in the Pacific sector of the Southern Ocean, *Deep Sea Res., Part II*, *47*, 3315–3338, 2000.

Frew, R., A. Bowie, P. Croot, and S. Pickmere, Macronutrient and trace-metal geochemistry of an in situ iron-induced Southern Ocean bloom, *Deep Sea Res., Part II*, *48*, 2467–2482, 2001.

Fung, I. Y., S. K. Meyn, I. Tegen, S. C. Doney, J. John, and J. Bishop, Iron supply and demand in the upper ocean, *Global Biogeochem. Cycles*, *14*, 697–700, 2000.

Gall, M. P., R. Strzepek, M. Maldonado, and P. W. Boyd, Phytoplankton processes, part 2: Rates of primary production and factors controlling algal growth during the Southern Ocean Iron Release experiment (SOIREE), *Deep Sea Res., Part II*, *48*, 2571–2590, 2001.

Gargett, A. E., Vertical eddy diffusivity in the ocean interior, *J. Mar. Res.*, *42*, 359–393, 1984.

Gregg, M. C., Diapycnal mixing in the thermocline: A review, *J. Geophys. Res.*, *92*, 5286–5429, 1987.

King, F. D., and A. H. Devol, Estimates of vertical eddy diffusion through the thermocline from phytoplankton nitrate uptake rates in the mixed layer of the eastern tropical Pacific, *Limnol. Oceanogr.*, *24*, 645–651, 1979.

Large, W. G., and S. Pond, Sensible and latent heat flux measurements in moderate to strong winds, *J. Phys. Oceanogr.*, *12*, 464–482, 1982.

Law, C. S., A. J. Watson, and M. I. Liddicoat, Automated vacuum analysis of sulphur hexafluoride in seawater; Derivation of the atmospheric trend 1970–1993 and potential as a transient tracer, *Mar. Chem.*, *48*, 57–69, 1994.

Law, C. S., M. I. Liddicoat, A. J. Watson, and T. Stanton, Sulphur hexafluoride as a tracer of biogeochemical and physical processes in an open-ocean iron fertilisation experiment, *Deep Sea Res., Part II*, *45*, 977–994, 1998.

Law, C. S., A. P. Martin, M. I. Liddicoat, A. J. Watson, K. J. Richards, and E. M. S. Woodward, A Lagrangian SF_6 tracer study of an anticyclonic eddy in the North Atlantic: Patch evolution, vertical mixing and nutrient supply to the mixed layer, *Deep Sea Res., Part II*, *48*, 705–724, 2001.

Ledwell, J. R., A. J. Watson, and W. S. Broecker, A deliberate tracer experiment in Santa Monica Basin, *Nature*, *323*, 322–324, 1986.

Ledwell, J. R., A. J. Watson, and C. S. Law, Evidence for slow mixing across the pycnocline from an open-ocean tracer-release experiment, *Nature*, *364*, 701–703, 1993.

Ledwell, J. R., A. J. Watson, and C. S. Law, Mixing of a tracer in the pycnocline, *J. Geophys. Res*, *103*, 21,499–21,529, 1998.

Lewis, M. R., W. G. Harrison, N. S. Oakey, D. Herbert, and T. Platt, Vertical nitrate fluxes in the oligotrophic ocean, *Science*, *234*, 870–873, 1986.

Lefevre, N., and A. J. Watson, Modelling the geochemical cycle of iron in the oceans and its impact on atmospheric CO_2 concentrations, *Global Biogeochem. Cycles*, *13*, 727–736, 1999.

Löscher, B. M., J. T. M. de Jong, H. J. W. de Baar, C. Veth, and F. Dehairs, The distribution of iron in the Antarctic Circumpolar Current, *Deep Sea Res., Part II*, *44*, 143–188, 1997.

Martin, A. P., K. J. Richards, C. S. Law, and M. I. Liddicoat, Horizontal dispersion of an anticyclonic mesoscale eddy, *Deep Sea Res., Part II*, *48*, 751–767, 2001.

Martin, J. H., and S. E. Fitzwater, Iron deficiency limits phytoplankton growth in the northeast Pacific subarctic, *Nature*, *331*, 341–343, 1988.

Maldonado, M. T., and N. M. Price, Influence of N substrate on Fe requirements of marine centric diatoms, *Mar. Ecol. Prog. Ser.*, *141*, 161–172, 1996.

Maldonado, M. T., P. W. Boyd, J. Laroche, R. Strzepek, A. Waite, A. R. Bowie, P. L. Croot, R. D. Frew, and N. M. Price, Iron uptake and physiological response of phytoplankton during a mesoscale Southern Ocean iron enrichment, *Limnol. Oceanogr.*, *46*, 1802–1808, 2001.

Nightingale, P. D., G. Malin, C. S. Law, A. J. Watson, P. S. Liss, M. I. Liddicoat, J. Boutin, and R. C. Upstill-Goddard, In situ evaluation of air-sea gas exchange parameterizations using novel and conservative tracers, *Global Biogeochem. Cycles*, *14*, 373–387, 2000.

Oakey, N. S., and J. A. Elliot, Dissipation within the surface mixed layer, *J. Phys. Oceanogr.*, *12*, 171–188, 1982.

Okubo, A., Oceanic diffusion diagrams, *Deep Sea Res.*, *18*, 789–802, 1971.

Pacanowski, R. C., and S. G. Philander, Parameterization of vertical mixing in numerical models of tropical oceans, *J. Phys. Oceanogr.*, *11*, 1443–1451, 1981.

Parslow, J. S., P. W. Boyd, S. R. Rintoul, and F. B. Griffiths, A persistent sub-surface chlorophyll maximum in the inter-polar frontal zone south of Australia: Seasonal progression and implications for phytoplankton-light-nutrient interactions, *J. Geophys. Res.*, *106*, 31,543–31,557, 2002.

Peters, H., M. C. Gregg, and J. M. Toole, On the parameterization of equatorial turbulence, *J. Geophys. Res.*, *93*, 1199–1218, 1988.

Polzin, K. L., J. M. Toole, and R. W. Schmitt, Finescale parameterizations of turbulent dissipation, *J. Phys. Oceanogr.*, *25*, 306–328, 1995.

Polzin, K. L., J. M. Toole, J. W. Ledwell, and R. W. Schmitt, Spatial variability and turbulent mixing in the abyssal ocean, *Science*, *276*, 93–96, 1997.

Quay, P., W. Broecker, R. Hesslein, and D. Schindler, Vertical diffusion rate determined by tritium tracer experiments in the thermocline and hypolimnion of two lakes, *Limnol. Oceanogr.*, *25*, 201–218, 1980.

Sigmon, D. E., D. M. Nelson, and M. A. Brzezinski, The Si cycle in the Pacific sector of the Southern Ocean: Seasonal diatom production in the surface layer and export to the deep sea, *Deep Sea Res., Part II*, *49*, 1747–1763, 2002.

Strang, E. J., and H. J. S. Fernando, Vertical mixing and transport through a stratified shear layer, *J. Phys. Oceanogr.*, *31*, 2026–2048, 2001.

Sunda, W. G., and S. A. Huntsman, Iron uptake and growth limitation in oceanic and coastal phytoplankton, *Mar. Chem.*, *50*, 189–206, 1995.

Sunda, W. G., and S. A. Huntsman, Interrelated influence of iron, light and cell size on marine phytoplanktonic growth, *Nature*, *390*, 389–392, 1997.

Takeda, S., Influence of iron availability on nutrient consumption ratio of diatoms in oceanic waters, *Nature*, *393*, 774–777, 1998.

Trull, T., S. R. Rintoul, M. Hadfield, and E. R. Abraham, Circulation and seasonal evolution of polar waters south of Australia: Implications for iron fertilisation of the Southern Ocean, *Deep Sea Res., Part II*, *48*, 2439–2466, 2001.

Upstill-Goddard, R. C., A. J. Watson, M. I. Liddicoat, and J. Wood, Sulphur hexafluoride and Helium-3 as seawater tracers: Deployment techniques and continuous underway analysis of SF6 and cryotrap EC-GC, *Anal. Chem.*, *249*, 555–562, 1991.

Vasholz, D. P., and L. J. Crawford, Dye dispersion in the seasonal thermocline, *J. Phys. Oceanogr.*, *15*, 695–712, 1985.

Wanninkhof, R., Relationship between wind speed and gas exchange over the ocean, *J. Geophys. Res.*, *97*, 7373–7382, 1992.

Wanninkhof, R., et al., Gas exchange, dispersion, and biological productivity on the west Florida shelf: Results from a Lagrangian tracer study, *Geophys. Res. Lett.*, *24*, 1767–1770, 1997.

Watson, A. J., P. S. Liss, and R. A. Duce, Design of a small-scale iron enrichment experiment, *Limnol. Oceanogr.*, *36*, 1960–1965, 1991.

Watson, A. J., D. C. Bakker, P. W. Boyd, A. J. Ridgewell, and C. S. Law, Effect of iron supply on Southern Ocean CO_2 uptake and implications for glacial atmospheric CO2, *Nature*, *40*, 730–732, 2000.

Zentara, S. J., and D. Kamykowski, Geographic variation in the relationship between silicic acid and nitrate in the South Pacific Ocean, *Deep Sea Res., Part A*, *28*, 455–465, 1981.

E. R. Abraham and C. S. Law, NIWA, Greta Point, P. O. Box 14-901, Kilbirnie, Wellington, New Zealand. (e.abraham@niwa.co.nz; c.law@niwa.co.nz)

M. I. Liddicoat, PML, Prospect Place, West Hoe, Plymouth PL1 3DH, UK. (m.liddicoat@mail.pml.ac.uk)

A. J. Watson, School of Environmental Sciences, University of East Anglia, Norwich NR4 7TJ, USA. (a.j.watson@uea.ac.uk)